Urban underlying surface modulates summertime thunderstorm processes and associated cloud-to-ground lightning activities

Tao Shi[1], Yuanjian Yang[2*], Gaopeng Lu[3], Zuofang Zheng[4], Yucheng Zi[3], Ye Tian[5], Lei Liu[2], Simone Lolli[6]

[1]School of Mathematics and Computer Science, Tongling University, Tongling, 244000, China
[2]Collaborative Innovation Center on Forecast and Evaluation of Meteorological Disasters, Nanjing University of Information Science and Technology, Nanjing, 210000, China
[3]School of Earth and Space Sciences, University of Science and Technology of China, Hefei, 241000, China
[4]Institute of Urban Meteorology, China Meteorological Administration, Beijing, 100000, China
[5]Beijing Meteorological Observation Center, Beijing, 100000, China.
[6]CNR-IMAA, Contrada S. Loja, 85050 Tito Scalo (PZ), Italy

Correspondence to: Prof. Yuanjian Yang (yyj1985@nuist.edu.cn)

Abstract. The urban underlying surface may have a significant impact on thunderstorm processes and lightning activities, but there is still a lack explanation of the mechanism. Through a comparative analysis of cloud-to-ground (CG) lightning location datasets in three cities of varying sizes, it was observed that for small cities, CG activities tend to cluster towards the city center, whereas, in large cities, CG activities were inclined to accumulate in the city periphery. Radar echoes indicated the occurrence of a significant barrier effect as the "0713" thunderstorm passed over Beijing's built-up area. An analysis of ground observations revealed that when this thunderstorm passed over the rough urban underlying surface, a separation of the near-surface cold pool emerged. This separation led to the weakening of vertical airflow and the breakdown of the convergence line, ultimately triggering the bifurcation and moving around of the thunderstorm. Numerical simulations have facilitated our further exploration into the potential mechanism of the barrier effect. When a portion of the built-up area was replaced with bare land, the separation of the cold pool and the breakdown of the convergence line were notably mitigated. Additionally, the building density could also influence the evolution of the cold pool and convergence line. Consequently, the urban underlying surface might be a potentially crucial factor affecting the thunderstorm processes and CG activities. This study would offer a fundamental foundation and technical support for predicting and assessing urban summertime thunderstorm disasters.

1 Introduction

As urbanization progressed, lightning events emerged as a significant hazard to city safety and social development, presenting a serious weather-related risk (Westcott & Nancy, 1995; Pinto et al., 2004). Among these events, CG lightning poses the greatest risk to both ground-based objects and populations. The scientific community has widely acknowledged the

consensus regarding the enhancement of the urban thermal effect on the thunderstorm processes (Shepherd, 2005; Wang et al., 2018; Yue et al., 2019; Wang et al., 2021; Shi et al., 2023). The thermal effect increases the boundary layer height above cities and the vertical mixing height (Xu et al., 2013; Sun et al., 2021). The vertical mesoscale cutting resulting from temperature differences between urban and suburban areas serves as a key prerequisite for the development of the convective system (Farias et al., 2014; Sun et al., 2013).

Previous studies have also recognized the dynamic effect of urban underlying surface on thunderstorm processes and lightning activities (Bornstein & LeRoy, 1990; Dai et al., 2005; Yang et al., 2021; Shi et al., 2023). The urban rough underlying surface can alter the horizontal wind field, enhancing convergence and upward movement in the upstream direction (Jin & Shepherd, 2005), which to some extent facilitates the development of thunderstorm systems (Yin et al., 2020). The intensity of airflow "climbing" movement is relatively weak (Zhu et al., 2016), and insufficient to alter the organization processes of thunderstorms. Moreover, researchers have also discovered that when thunderstorms pass over the cities, the dynamic effect of the urban underlying surface can lead to the bifurcation and moving around of thunderstorm systems (Bernstein & LeRoy, 1990; Lorenz et al., 2019). This process inhibits the development of thunderstorms over the city center, resulting in the concentration of lightning and rainfall in the city periphery, a phenomenon known as the barrier effect (Stallins & Bentley, 2006). In the characterization of the urban underlying surface, city size is recognized as a crucial factor that impacts thunderstorm processes (Kingfield et al., 2018). Additionally, the building density also demonstrates a tendency to alter urban lightning activities (Stallins & Bentley, 2006).

With a population exceeding 20 million, a built-up area spanning approximately 1500 km^2, and a gross domestic product (GDP) exceeding 4 trillion, the Beijing megacity stands as the most urbanized city within the urban agglomeration of Beijing-Tianjin-Hebei (National Bureau of Statistics of the People's Republic of China, 2021). In recent years, the Beijing megacity has been repeatedly impacted by severe convective events, leading to significant economic and social disruptions (Qie et al., 2021). Some studies analyzing thunderstorms passing over Beijing megacity have found that the urban barrier effect primarily dominates the thunderstorm processes (Dou et al., 2015; Shi et al., 2023). However, other researcher pointed out that, despite the buildings in the Beijing megacity splitting the squall line into convective cells, the barrier effect on convection is less significant compared to the thermal effect (Miao et al., 2011). In general, there is ongoing debate regarding the dominant role of Beijing's urban underlying surface on summertime thunderstorm processes, with the potential thermodynamic mechanisms remaining the gap in research.

To address these issues, this study focused on the Beijing megacity as the main research area, utilizing radar echo data and lightning location data to analyze the organization processes and the spatial patterns of CG activities during thunderstorms passing over the city. Subsequently, numerical simulations were employed to explore the mechanisms by which the urban underlying surface influenced the evolution of the thermodynamic structure of thunderstorms. Our present work aims to contribute valuable theoretical insights and technical support to enhance the prediction, nowcasting, warning, and risk assessment capabilities for urban thunderstorm disasters.

2 Data and methodology

2.1 Study Area

Beijing megacity serves as the political, economic, cultural, and scientific center of China. With a dense population and rapid urbanization, the built-up area of Beijing has expanded to more than 1500 km², covering most of the southeastern plain regions (as shown in Figure 1). Thunderstorms in Beijing typically originate from the western mountains and spread to the northeast and southeast plains (Chen et al., 2012a). When interacting with warm and humid airflows southward, these thunderstorms often intensify and form squall lines (Sun & Yang, 2008; Xiao et al., 2017). Zhangjiakou and Tianjin are located in the northwest and southeast of Beijing, respectively. Both regions show a similar climate to Beijing, characterized by a temperate continental monsoon climate with frequent thunderstorms during summer. Zhangjiakou is located approximately 180 km from Beijing, with a built-up area of 104.2 km², only one-tenth of the built-up area of Beijing. It is considered to be one of the least urbanized cities within the Beijing-Tianjin-Hebei urban agglomeration. In comparison, the built-up area of Tianjin, situated just 60 km from Beijing, spans approximately 605.42 km². Beijing, Zhangjiakou, and Tianjin show different urbanization levels. For this reason, they were used to explore the effects of urban underlying surface on lightning and storm processes.
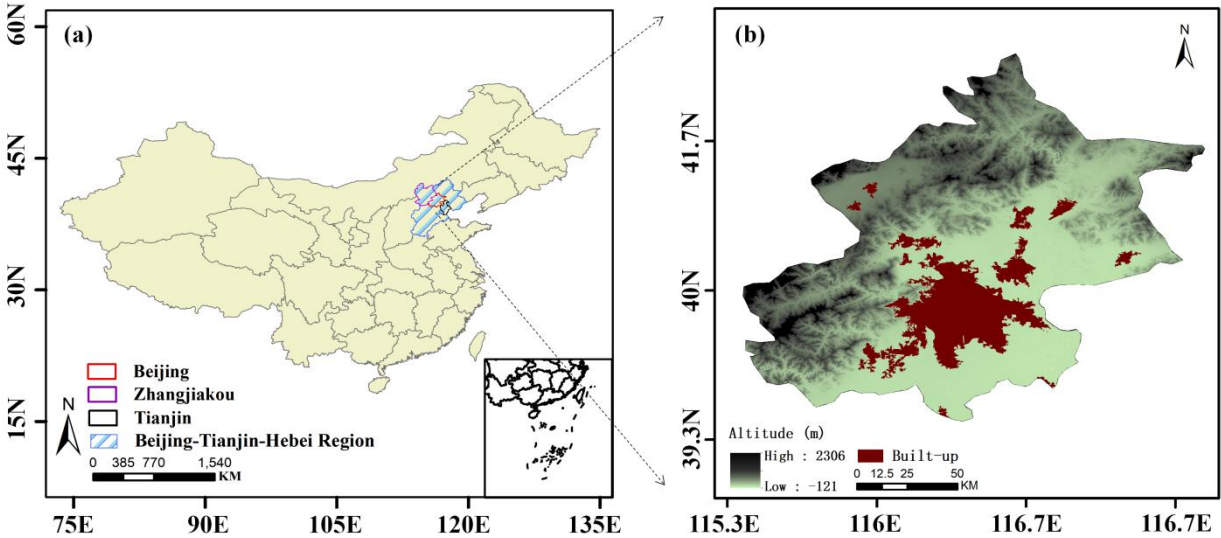
Figure 1: Overview of the study area (a). Topography and built-up area in Beijing megacity (b).

2.2 Data

The State Grid Lightning Network (SGLNET) is utilized to collect lightning location datasets, which include longitude and latitude, GPS time, peak current, polarity, and other relevant information (Wang et al., 2021). Lightning events are detected using magnetic direction-finding and time-of-arrival (MDF-TOA) technologies within the SGLNET, achieving a detection

efficiency of 94% and a location error of 489 m, respectively (Chen et al., 2012a). A previous study by Orville et al. (2002) pointed out that intra-cloud (IC) discharges may contaminate the CG lightning detection network. To address this issue, we used a screening criterion based on a peak current threshold of less than 10 kA to eliminate the potential interference from IC discharges (Schulz et al., 2005). In this study, the SGLNET lightning location data from the summer months (June to August) between 2010 and 2017 were selected to analyze the characteristics of urban CG lightning activities.

The hourly observation data from the auto weather station (AWS) utilized in this study were obtained from the China Meteorological Data Service Center (http://data.cma.cn/en). This dataset included near-surface air temperature, wind speed, and wind direction. To address missing values in the observation sequence, we used a method previously described by Yang et al. (2011). Specifically, we replaced missing values with the average of synchronous observation data from the nearest five stations, and stations with excessive erroneous records were excluded. For this study, we selected 54 AWSs, which are evenly distributed throughout the built-up area of Beijing, to analyze the temporal-spatial pattern of the near-surface thermal-dynamic field.

Doppler Radar Data. This radar observation system consists of a data acquisition subsystem, a product generation subsystem, and a main user terminal subsystem. It enables real-time data transmission and image stitching, significantly boosting the monitoring and early warning capabilities for disastrous weather conditions such as severe convective weather, tropical cyclones, and heavy rainfall. The radar data employed in this paper is the Composite Reflectivity (CR) product generated by the S-band Doppler Radar stationed at the Beijing Nanjiao Observatory. Previous studies have consistently recognized a threshold of 35 dBZ as a pivotal marker signifying the presence of a convective echo (Dixon & Wiener, 1993; Roberts & Rutledge, 2003; Mecikalski & Bedka, 2006). Consequently, this research adopts this well-established reflectivity threshold as the criterion for identifying thunderstorms. In addition, to gain a broader understanding of the synoptic background of thunderstorms, we utilized sounding data from the Beijing Nanjiao Observatory. These sounding data were collected at 02:00, 08:00, 14:00, and 20:00 Beijing time every day.

Stewart & Oke (2012) introduced the concept of local climate zone (LCZ) datasets, which refer to areas with identical land use, similar spatial morphology, building materials, and human activities, on a scale ranging from a few hundred to a few thousand meters. The LCZ datasets used in this paper were provided by the Institute of Urban Meteorology, China Meteorological Administration (as shown in Figure S1). Detailed descriptions and attribute parameters of categories of LCZ datasets were presented in Table S1.

2.3 Numerical simulation scheme

Currently, the Weather Research and Forecasting (WRF) model holds a prominent position as the primary tool for simulating urban environments. The WRF model, collaboratively developed by institutions such as the National Center for Atmospheric Research (NCAR) and the National Centers for Environmental Prediction (NCEP) in the United States, is primarily designed for operational forecasting and atmospheric research. This model enables researchers to simulate real-world or hypothetical

scenarios computationally, offering a highly flexible and efficient predictive framework that can be applied to studies examining the impacts related to urban meteorology (Chen et al., 2012b). The WRF model, when coupled with the Urban Canopy Model (UCM), is employed to describe the dynamic, thermal, and radiative interactions between urban land surface processes and the upper atmosphere (Kusaka et al., 2001; Chen et al., 2012b). The UCM not only accounts for the geometric measurements of urban buildings and roads but also optimizes the physical parameters of urban canopies. Furthermore, it calculates heat transfer across building roofs, walls, and road surfaces. The UCM is widely utilized in studies examining atmospheric boundary layer processes and environmental issues related to urbanization (He et al., 2019).
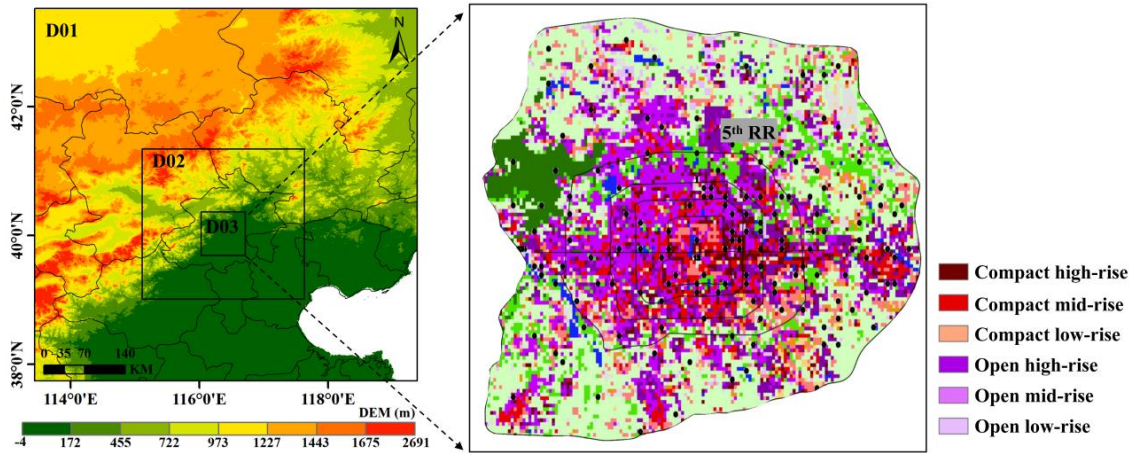
Figure 2: Terrain height distribution and the building types of the WRF mesoscale numerical model.

In this study, the WRF 4.0 version, integrated with UCM, was configured to use a triple-nested grid system with horizontal resolutions of 5 km, 1 km, and 200 m, respectively (Figure 2). The model center is located at (40.0°N, 116.6°E), with grid dimensions of 515×151, 256×251, 506×501, and 38 vertical layers. The underlying surface data encompassed land use and urban canopy datasets with a resolution of 10 m. This model employed the WRF Single Moment 6-class microphysical process scheme (WSM6), the rapid radiative transfer longwave radiation scheme (RRTM), the Dudhia shortwave radiation scheme, the step-mountain similarity theory near-surface layer scheme, and the BouLac boundary layer scheme (Lim & Hong, 2010; Iacono et al., 2008; Janjic, 1994; Melin et al, 2017; Tewari et al., 2004). The simulation began at 00:00 on July 13th, 2017, and lasted for 24 hours. The length and area of the 5th Ring Road (RR) in Beijing are approximately 98.6 km and 600 km^2, respectively. To more accurately assess the impact of urban underlying surface on the dynamic and thermal effects, we conducted five sets of experiments. These included a control experiment (EXP1) and four sensitivity tests (EXP2, EXP3, EXP4, EXP5). The specifics of these experiments are described in Table 1.

Table 1: Description of different experiments.

Experiment	Style	Description
EXP1	Controlled experiment	Actual land use situation and building structure
EXP2	Sensitive experiment	Outside the 5th RR with only bare land
EXP3	Sensitive experiment	The built-up area with only bare land
EXP4	Sensitive experiment	The built-up area with only open-rise
EXP5	Sensitive experiment	The built-up area with only compact-rise

3 Results

3.1 CG activities around the built-up area

Spatial analysis of long-term lightning location data offers valuable insights into the climatic patterns of CG activities, which constitutes a crucial component of urban thunderstorm disaster research. In this section, a thorough examination of the spatial characteristics of CG activities was conducted in the built-up area of Beijing using SGLNET data.
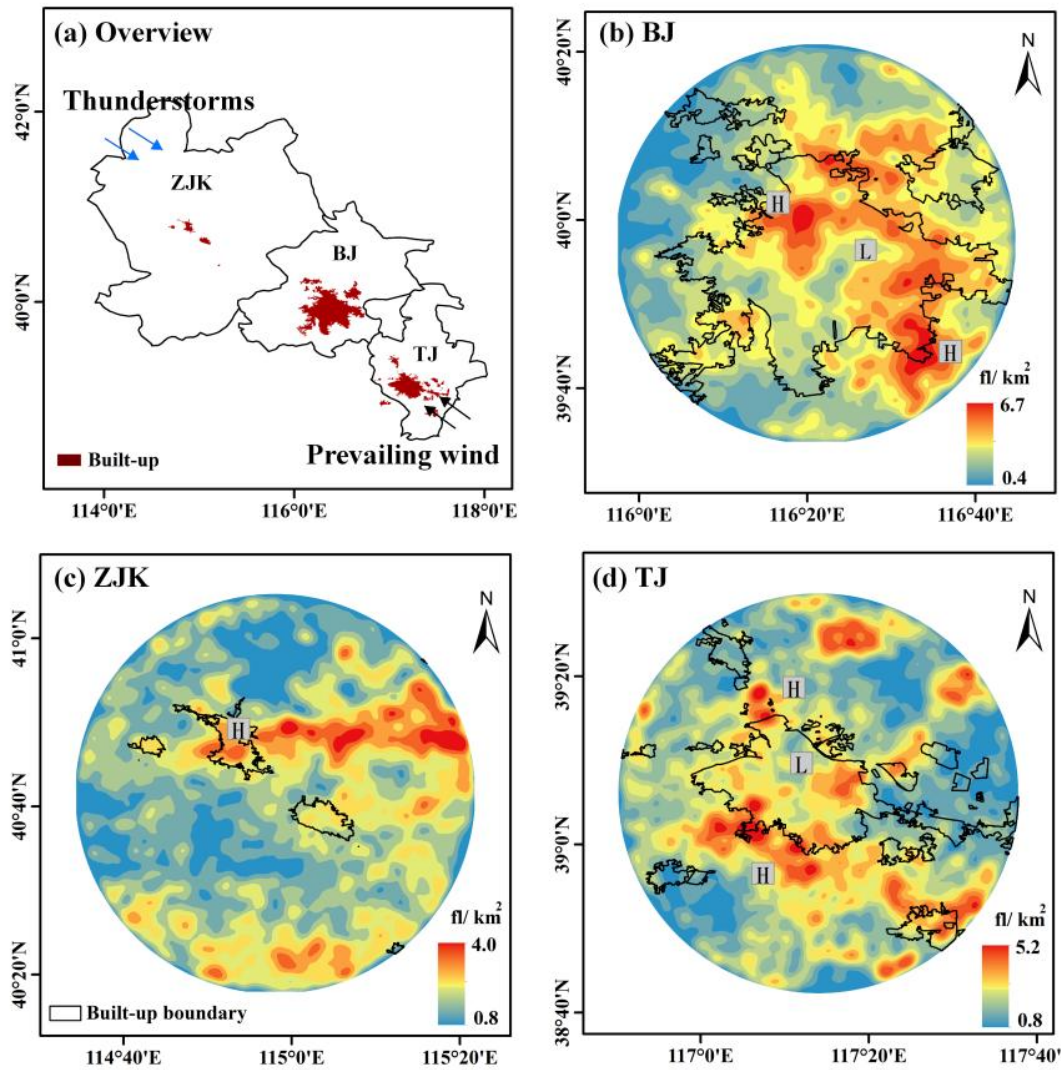
Figure 3: Overview of the built-up areas in Beijing (BJ), Zhagnjiakou (ZJK), and Tianjin (TJ) (a). Spatial patterns of CG density in the built-up areas of Beijing (b), Zhangjiakou (c), and Tianjin (d) during the summertime of 2010-2017.

The locations and built-up area scales of Beijing, Zhangjiakou, and Tianjin are illustrated in Figure 3a. SGLNET recorded more than 50,000 CG flashes in the built-up area of Beijing during the study period. It is clear that the distribution of CG density in the built area of Beijing was uneven (Figure 3b). There were clusters of abundant CG flashes visible and concentrated upwind and downwind of the built-up area (marked as H), with an average and maximum CG density reaching 4 fl/km^2 and 6 fl/km^2, respectively. It should be noted that the CG flashes in the city center were sparse (marked as L), with an average CG density of less than 1 fl/km^2. This pattern was similar to the spatial distribution of CG flashes observed in the United States, more precisely in Houston (Steiger & Orville, 2002) and Atlanta (Stallins & Bentley, 2006). Therefore, we

could speculate that there existed a potential barrier effect that alters the pattern of CG lightning in the built-up area of Beijing. As shown in Figure 3c, the entire built-up area of Zhangjiakou (ZJK) was mainly covered by a high CG density (H) region, with a peak density of 3.6 fl/km^2 in the city center. Examining Figure 3d, it was evident that a significant concentration of CG lightning occurs along the outskirts of the built-up area of Tianjin (TJ), with a maximum CG density of 5.2 fl/km^2. Similar to Beijing, the center of the built-up area in Tianjin exhibited a low CG density (L) region. Thus, this paper could infer that under similar climatic conditions, the larger the built-up area, the lower the CG density in the city center.

This section summarized the spatial distribution of CG density and various LCZs in Beijing, aiming to understand the relationship between CG activities and the urban underlying surface. As illustrated in Figure S2, there were 3,525 pixels in LCZ1, 4,699 pixels in LCZ2, and 4,486 pixels in LCZ3, accounting for 10.5%, 14.0%, and 13.4% of the built-up area, respectively. The average CG density in these zones was 3.7 fl/km^2, 3.5 fl/km^2, and 3.0 fl/km^2, respectively. Furthermore, there were 7,262 pixels in LCZ4, 10,466 pixels in LCZ5, and 3,027 pixels in LCZ6, representing 21.7%, 31.3%, and 9.1% of the built-up area, respectively. The average CG in these zones was 3.6 fl/km^2, 3.3 fl/km^2, and 2.8 fl/km^2, respectively. It was evident that in both the compact-rise (LCZ1, LCZ2, LCZ3) and open-rise (LCZ4, LCZ5, LCZ6) areas, the density of CG increased as the height of the building increased.
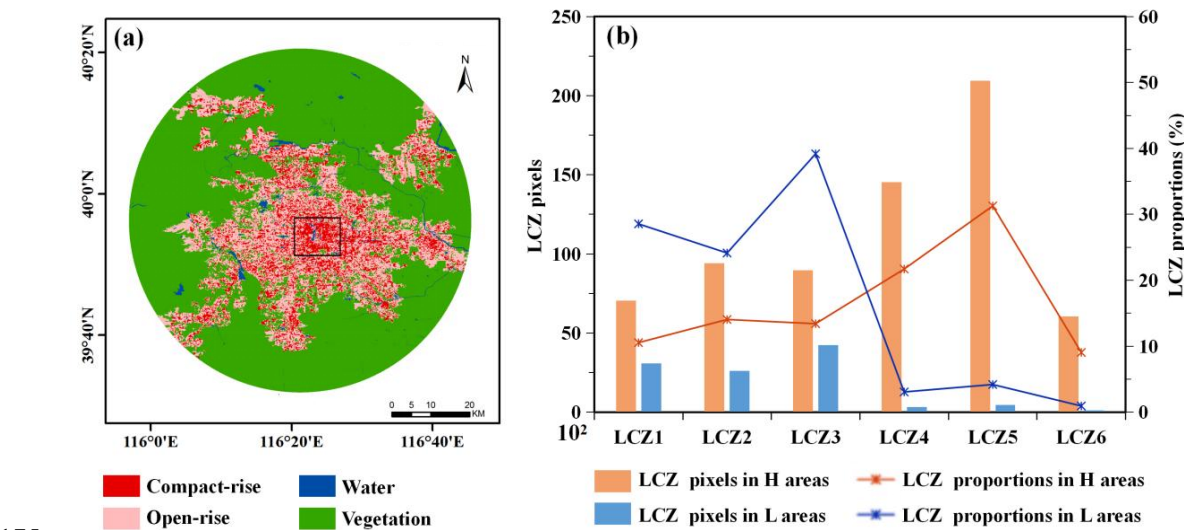
Figure 4: (a) Characteristics of the urban configuration structure dominated by density information, including compact-rise (LCZ1, LCZ2, LCZ3) and open-rise (LCZ4, LCZ5, LCZ6). (b) The configuration structure of buildings in areas with high CG density (H) and low CG density areas (L).

The impact of building density on CG activities also could not be ignored. Stallins & Bentley (2006) used GIS technology to analyze the distribution characteristics of lightning in Atlanta USA, and discovered that the lightning density was low in high-density building areas. In Figure 4a, density information was used as the dominant factor to classify the urban configuration structure, which was divided into compact rise (LCZ1, LCZ2, LCZ3) and open rise (LCZ4, LCZ5, LCZ6). The

edges of the built-up area in Beijing are primarily composed of open rise. The city center is completely constituted of compact rise, forming large-scale compact rise clusters with an area of approximately 100 km² (depicted in the black box), which was largely congruent with the low CG density areas within the built-up area. Figure 4b illustrates the distribution of various LCZs in the high CG density areas (H) and low CG density areas (L). The H areas were primarily located in the upper and lower wind directions, spanning over 1000 km². Among these areas, the LCZ5 was the largest building type, comprising 14,524 pixels, and representing 31.2% of the total H areas. The areas of other LCZs were relatively similar, accounting for 11.05%~21.2%. The L areas were primarily concentrated in the city center, spanning a total area of approximately 90 km². This area comprised 9,936 dense pixels, representing 91.8% of the total L areas. The L areas were mainly composed of compact rise and contained very few open rise. Consequently, the city size and building density might be important factors affecting CG activities.

3.2 The evolution of the thunderstorm passing over the underlying urban surface

The CR product detected by the Beijing Nanjiao Observatory was utilized to analyze the evolution of thunderstorms passing over the built-up area. Figure 5a depicted the "0713" case, a quasi-linear convective system consisting of multiple cells that propagated from Hebei at 20:00 Beijing time (BJT). At this time, the thunderstorm system reached the northwest of the built-up area. Thunderstorm cells were continuously generated, developed, and merged on the right rear side of the thunderstorm system. At 21:00 BJT (Figure 5b), the thunderstorm moved to the border between the mountains and the plain and there was an evident V-shaped notch on its rear side, indicating a robust rear inflow. The area of the strong echo above 40 dBZ expanded further, with the echo center intensity peaking at more than 50 dBZ. It was important to note that during its propagation, the thunderstorm system broke down and gradually split into larger thunderstorm cell I and smaller thunderstorm cell II in the northwest corner of the built-up area, emerging a significant barrier effect.
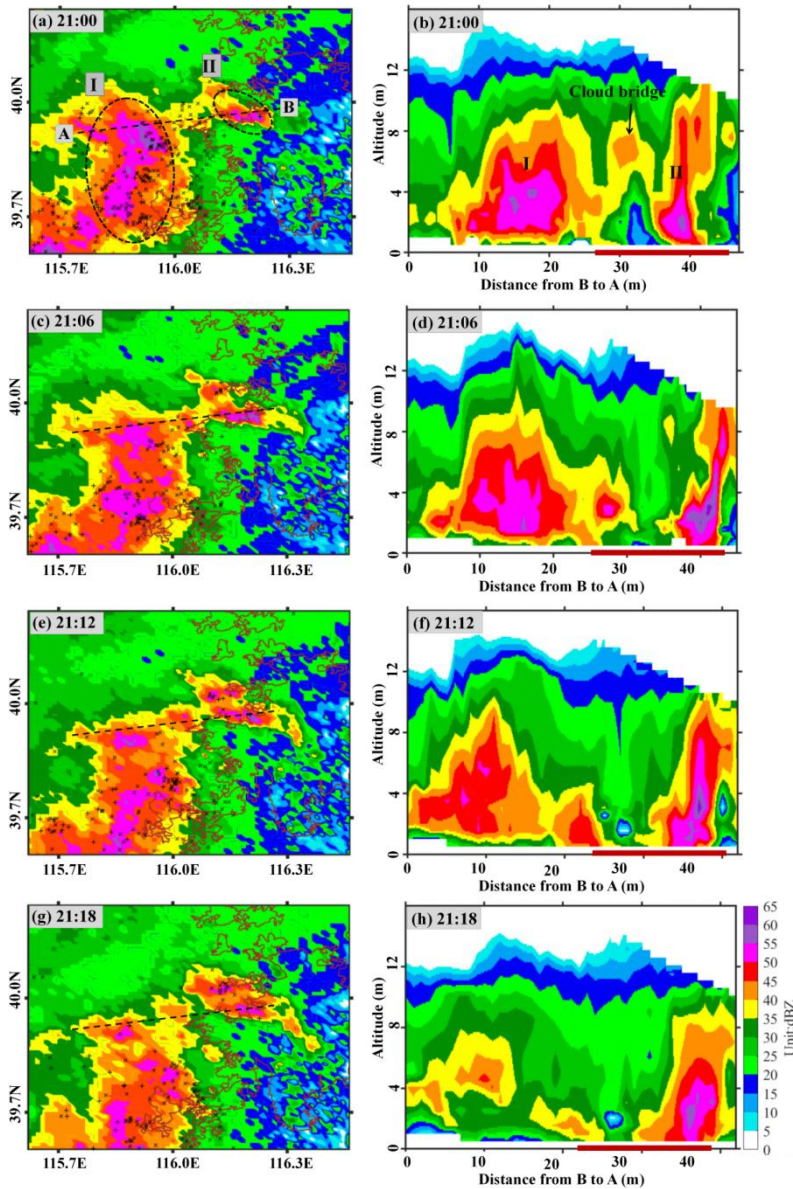
Figure 5: The CR product of the case "0713" during the stage of bifurcation, at 21:00 (a-b), 21:06 (c-d), 21:12 (e-f), and 21:18 (g-h) BJT.

Due to the barrier effect, the thunderstorm system began to split, with cell I and cell II remaining connected by a cloud bridge. At 21:06 BJT (Figure 5c-6d), the echo core volume of cell I decreased, and the cloud bridge began to narrow. The echo core height of cell II expanded to 8 km, with a maximum reflectivity exceeding 65 dBZ. Furthermore, newborn cells emerged around the cloud bridge. By 21:12 BJT (Figure 5e-6f), as the thunderstorm system approached the built-up area, the echo core of cell I and the cloud bridge weakened to 45 dBZ, while the echo core height and strong echo area of cell II continued to increase. At 21:18 BJT (Figure 5g-5h), cell I and cell II were completely separated when the cloud bridge broke.

Therefore, during the "0713" case passing over the built-up area of Beijing, the urban underlying surface directly affected the spatial pattern of CG activities and the organization process of the "0713" case.
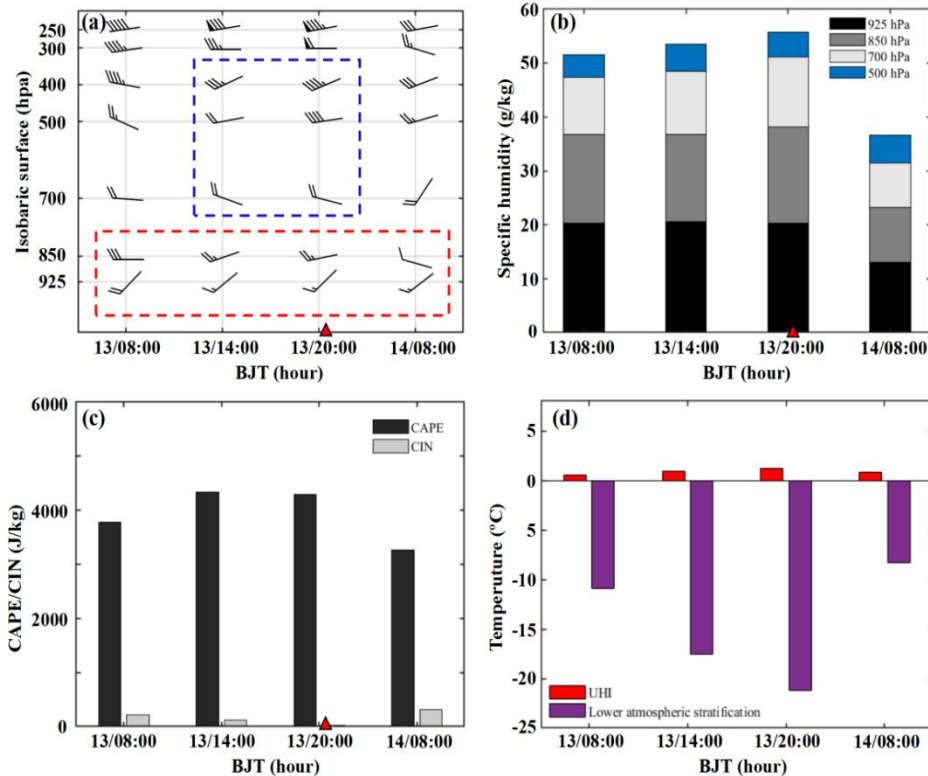
Figure 6: Wind field (a), specific humidity (b), convective effective potential energy (CAPE) and convective inhibition energy (CIN) (c), urban heat island (UHI) intensity and lower atmospheric stratification (d). The red triangle represents the time when the "0713" case passed over the built-up area.

Through observational data, in this study, we analyzed in detail the variation of the thermal-dynamic field of the "0713" case passing over the built-up area. At 08:00 BJT (Beijing time), the wind direction below 850 hPa in the built-up area varied clockwise with height (red box in Figure 6a), indicating a small amplitude and weak warm advection in the lower atmosphere. The urban heat island (UHI) intensity and the pseudo-equivalent temperature between 850hPa and 925 hPa were 0.5°C and −10.9°C, respectively, indicating unstable atmospheric stratification in the lower atmosphere. In Figure 6b-6c, the specific humidity at 850 hPa exceeded 20 g/kg, indicating a rich water vapor content. Specific humidity at 500 hPa was approximately 4 g/kg, demonstrating the characteristics of the upper dry and lower wet vertical water vapor layer. The convective available potential energy (CAPE) value reached 3783.5 J/kg. At 14:00 BJT, the wind field in the middle and upper levels changed counterclockwise with height (shown in the blue box in Figure 6a), representing a strong cold advection passing over the city. As the thunderstorm system moved into the built-up area, the configuration of upper cold and lower warm increased atmospheric stratification instability. Although the UHI intensity in the built-up area was only

230 0.8ºC (Figure 6d), the pseudo-equivalent temperature between 850 hPa and 925 hPa decreased to −17.5ºC, and the CAPE value exceeded 4000 J/kg. By 20:00 BJT, the UHI intensity, pseudo-equivalent temperature, and CAPE value continued to rise, leading to numerous CG lightning events initiated in the city periphery.
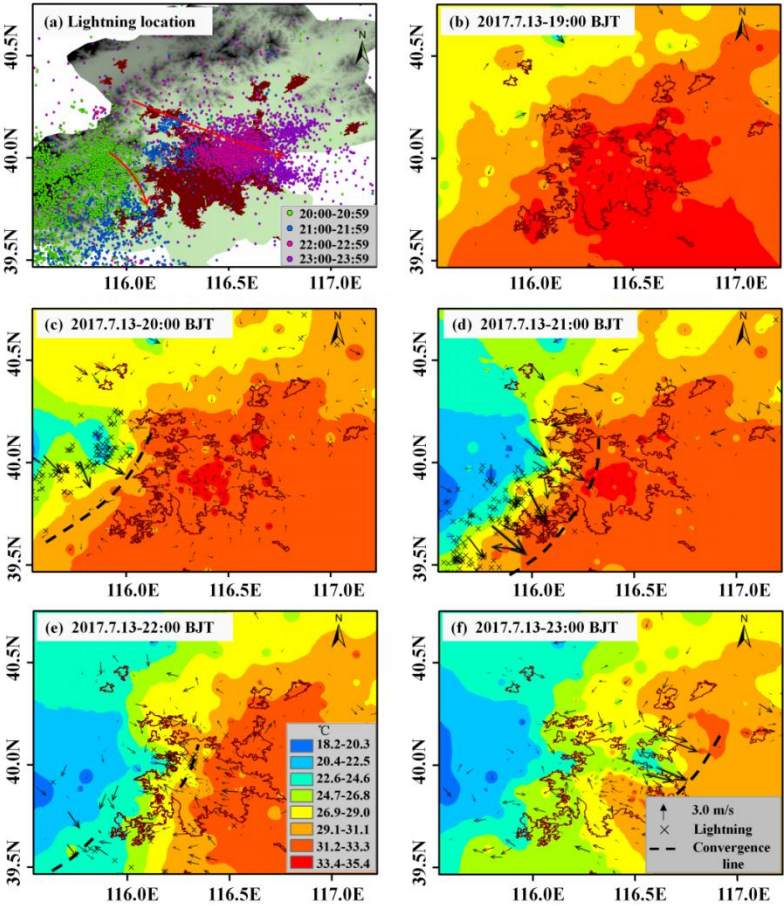
Figure 7: (a) The spatial pattern of CG activities. The dots represent cloud-to-ground lightning, and the red line represents the
235 **movement trajectory of the thunderstorm. (b-f) The near-surface thermal-dynamic fields of the "0713" case passing over the built-up area.**

Figure 7a illustrates the movement trajectory of the "0713" case and the monitoring results of CG activities. At 19:00 BJT (Figure 7b), the entire plain area of Beijing was dominated by a large-scale warm and humid south airflow. The warmest
240 center was located within the built-up area, exhibiting a UHI intensity of approximately 1.2ºC. At 20:00 BJT (Figure 7c), the squall line system originating from Taihang Mountain began to enter the northwest edge of the built-up area, creating a cold pool on the ground. The maximum wind speed at the front of this cold pool reached 7.1 m/s. A distinct convergence line was observed between the outflow boundary of the cold pool and the southerly winds of the environmental field in the west of the built-up area. This convergence line followed a northeast-southwest trajectory overall. The convergence zones triggered

245   strong vertical upward movement of airflow in the lower layer, leading to 337 CG events in areas where the temperature gradient zones were most pronounced. At 21:00 BJT (Figure 7d), as the thunderstorm system developed eastward, the cold pool area expanded further. The maximum wind speed at the front of the cold pool reached 10.4 m/s, and 417 CG events occurred around temperature gradient zones. It was worth noting that at this time the outflow boundary became bifurcated at the edge of the built-up area, and the convergence line began to fragment. At 22:00 BJT (Figure 7e), the outflow angle of the

250   cold pool expanded further. Under the influence of the bifurcated airflow, two cold tongues emerged on the west side of the built-up area. The convergence line broke completely, leading to a significant barrier effect. At this time, SGLNET only recorded 54 CG flashes near the split convergence line. At 23:00 BJT (Figure 7f), the thunderstorm cell continued to propagate in the built-up area, and SGLNET registered 181 CG events within the built-up area.

Based on the above analysis, when the thunderstorm passed over the built-up area, it exhibited a bifurcated process due to

255   the barrier effect. Utilizing this pattern as a screening criterion, we categorized thunderstorms passing over the built-up area of Beijing from 2010 to 2017 into bifurcated thunderstorms (BT) and non-bifurcated thunderstorms (NBT). According to Figure S3, the year with the highest number of BT was 2013, with eight events, accounting for 23.5% of the total thunderstorms; the lowest number of BT was observed in 2010, with two events, representing 15.4% of the total thunderstorms. These results indicated that the barrier effect of urban underlying surface was a prevalent phenomenon in

260   long-term thunderstorm observations. Furthermore, as the thunderstorm passed over the built-up area, the evolution of near-surface cold pools and convergence lines could serve as diagnostic indicators to understand how the urban underlying surface affected the thunderstorm process and CG activities.

3.3 Numerical simulation of the influence of urban underlying surface on the thermal-dynamic structure of thunderstorms

265   This section made a comparison between the observed values of AWS around the built-up area and the simulated values derived from the control experiments to verify the simulation accuracy.

Figure S4 illustrates the simulation accuracy of hourly meteorological elements. As the thunderstorm system progressed towards urban areas (specifically at 20:00 BJT), AWS documented a decrease in air temperature accompanied by an increase

270   in air pressure. At 22:00 BJT, there was a notable increase in air pressure, a sharp drop in air temperature, and a concurrent rapid increase in wind speed. The simulated pressure exhibited a trend similar to that of the observed pressure, with the simulated pressure being 2.1 hPa lower than the observed pressure at 17:00 BJT. The curve of the simulated temperature showed a slight lag compared to that of the observed temperature. The variation in simulated wind speed closely mirrored that of the observed temperature, with both showing a rapid increase after 20:00. The emergence of these simulation errors

275   could potentially be attributed to the chosen physical scheme, along with the initial and boundary conditions that were imported. On an overall basis, the simulated ground meteorological fields were able to adequately capture the near-surface thermodynamic characteristics associated with the "0713" case.
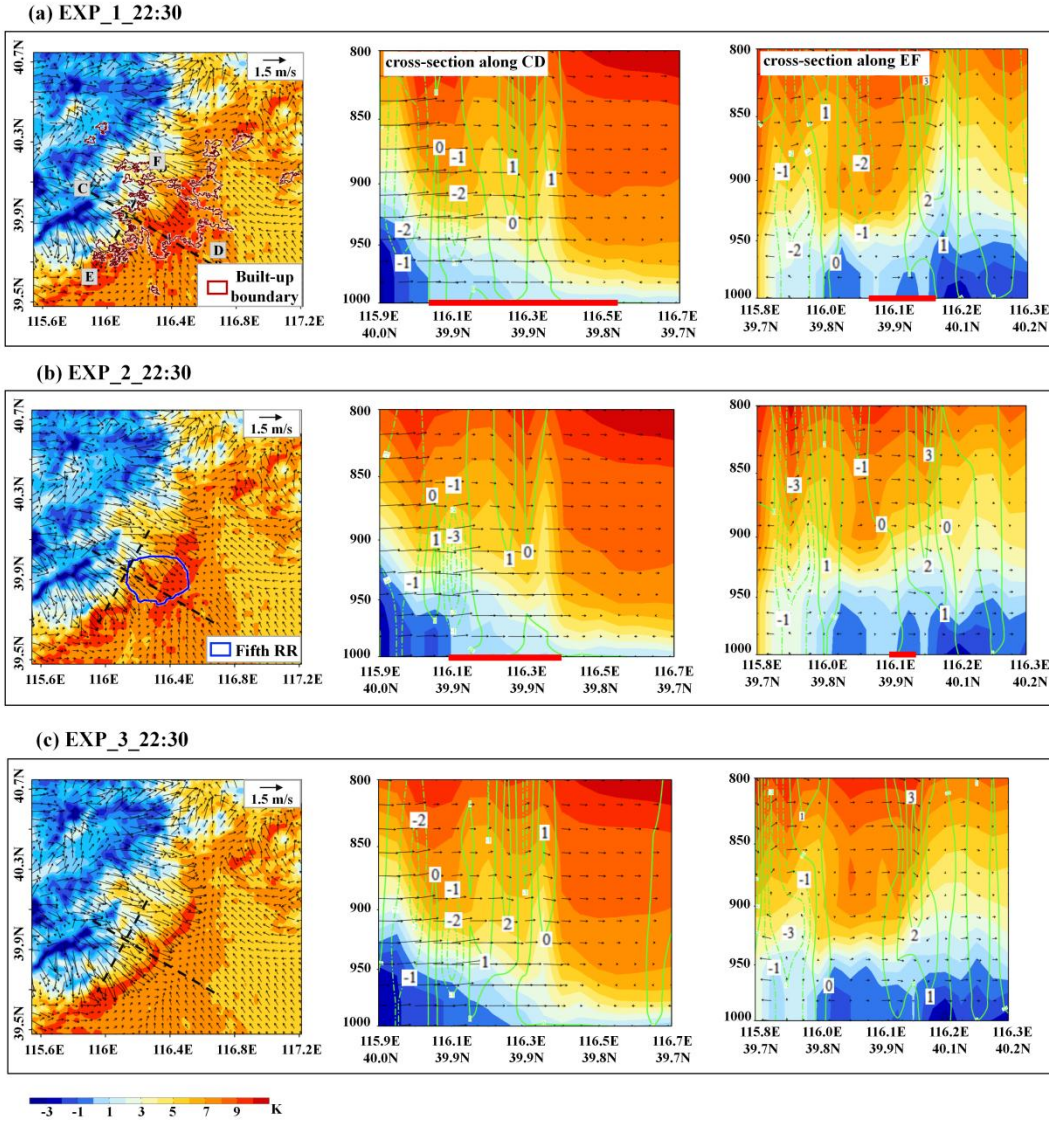
Figure 8: Influence of the scale of the built-up area on near-surface cold pool outflow simulated by WRF. Figures (a) to (c) represent experiments 1 to 3, respectively. In each set of subfigures, the left subfigure represents the horizontal thermal-dynamical field, and the middle and right subfigures depict the cross-sections along line CD and EF respectively, including perturbation potential temperature (shaded), east-west circulation (vector), and vertical velocity (isoline).

Referring to previous research (Takemi, 2006; Yuan, 2015), this paper used a criterion of a perturbation potential temperature lower than −1 K to define the core of the cold pool. The density flow outside this core, which spans a range of −1 K to 1 K, was also defined. In the experiment 1 (Figure 8a), the simulation results showed that at 22:30 BJT, as the dry cold air sank and spread, the intensity of the near-surface cold pool increased. The minimum perturbation potential temperature of the cold pool core reached −3 K. It became evident that as the cold pool approached the edge of the built-up

area, the outflow on both sides of the city moved faster, representing that the urban underlying surface dragged the cold pool.

290 A cross-section along the line CD revealed that due to the barrier effect of the underlying surface, the cold pool accumulated at the city periphery, with a core thickness of approximately 0.5 km. The urban underlying surface altered the motion of the cold pool, making the cold pool unable to maintain a smooth and continuous shape, and then it bifurcated. A cross-section along line EF revealed that the cold pool was divided into three relatively independent cores, with a more significant thickness at the edge of the city compared to its inner regions. The length and area of the built-up area in Beijing are

295 approximately 98.6 km and 600 km^2, respectively. In the experiment 2 (Figure 8b), buildings outside the 5th Ring Road were replaced with bare land, which weakened the accumulation of the cold pool, resulting in a thickness of less than 0.4 km. This led to an increase in vertical speed over the city center, mitigating the separation of the cold pool. When all built-up areas were replaced with bare land in experiment 3 (Figure 8c), the accumulation of cold pool cores disappeared. The cold pool cores exhibited a complete and continuous shape, with vertical upward movement continuing to increase, and the barrier

300 effect almost disappeared.
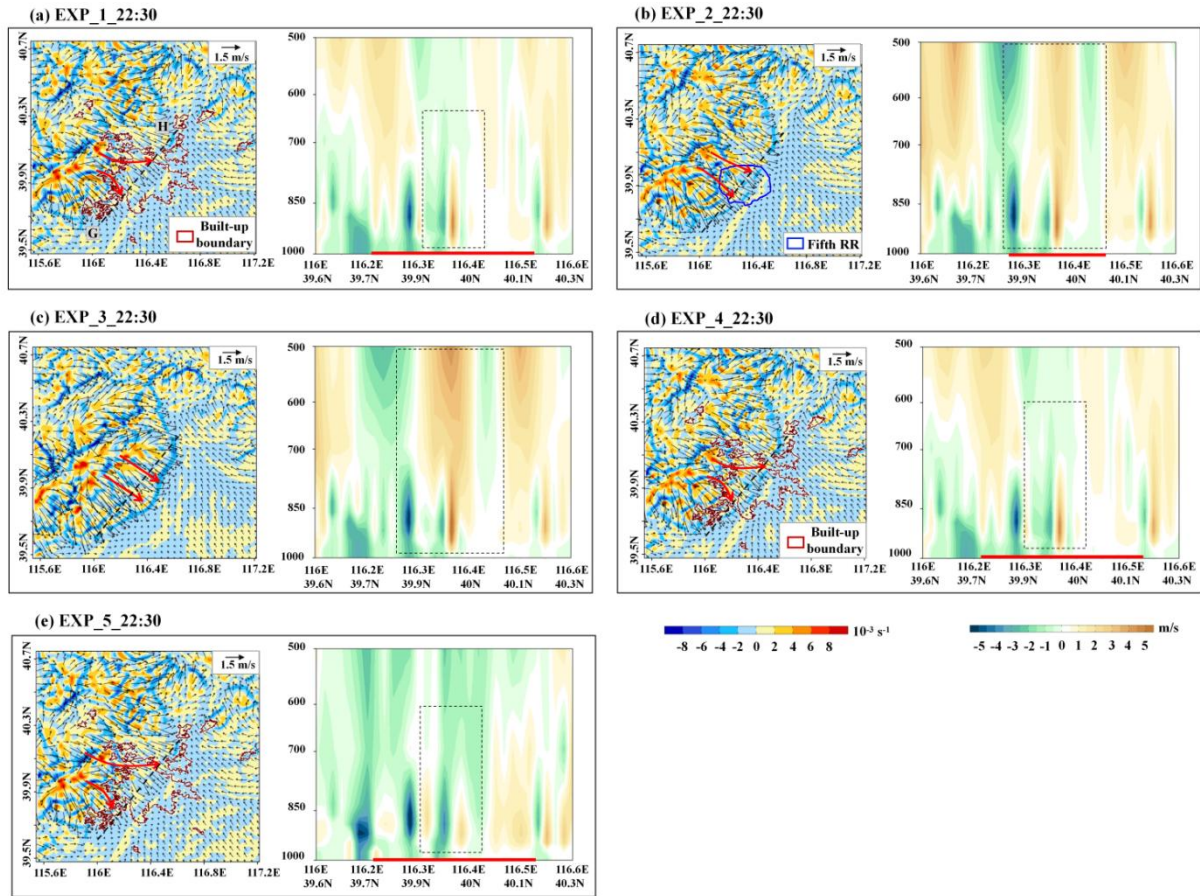
Figure 9: Influence of urban underlying surface on near-surface convergence zones simulated by WRF. Figures (a) to (e) represent experiments 1 to 5, respectively. In each set of subfigures, the left subfigure represented the horizontal wind field and divergence field, while the right subfigure depicted the cross-section of vertical velocity along line GH.

305

In EXP1 (Figure 9a), the horizontal field showed that the maximum wind speed at the front of the cold pool outflow reached approximately 5 m/s. Here, the outflow boundary of the cold pool converged with the southerly winds of the environmental field, while divergence zones formed at the city center. The gust front at the exit of the cold pool exhibited bifurcation, with one segment southward and the other northward, leaving a sparse outflow in the middle. The cross-section illustrated that the

310 vertical ascending zone above the city center (denoted by the black dotted rectangle) aligned with the middle segment of the cold pool outflow, though its range and intensity were smaller compared to those in the city periphery. In contrast, under the conditions of EXP2 (Figure 9b), where the roughness of the urban underlying surface was diminished, the cold pool outflow exhibited a slight bifurcation. This resulted in relatively intact convergence zones within the built-up area. The vertical ascending zone over the city center expanded in range, with a maximum vertical velocity reaching about 4 m/s. In EXP3

315 (Figure 9c), the maximum wind speed at the front of the cold pool outflow surpassed 8 m/s. The cold pool outflow completely traversed the built-up area, leading to a further enhancement of the range and intensity of the convergence zones, with a vertical velocity of 5 m/s. The above results showed that the scale of the built-up area could directly alter the strength of the barrier effect. Next, this section then further investigated the impact of building density on the barrier effect. In EXP4 (Figure 9d), all types of buildings were designated as open rise. Examination of the simulated dynamic field revealed that the

320 bifurcation angle, the structure of the convergence zone, and the vertical velocity of the cold pool outflow were largely consistent with those observed in EXP1. In EXP5 (Figure 9e), all types of buildings were set as compact rise. In particular, the separation angle of the cold pool outflow was larger than in EXP1, and the vertical velocity was smaller, indicating a more significant barrier effect. Therefore, it became evident that when summer thunderstorm passed over the city, the specific morphological characteristics of the underlying surface could significantly modulate the thunderstorm process.

4 Discussion

325

This section discussed the modulation of urban underlying surface on the thunderstorm processes and CG activities, focusing on the thermal-dynamic fields in the middle and lower layers.

As Figure 10a revealed, when thunderstorms passed over the small-scale city dominated by open rise, the barrier effect of the urban underlying surface on the dynamic field was constrained. The horizontal temperature gradient between the cold

330 pool outflow and the underlying surface generated vertical shear of wind speed (Weisman et al., 1984; Chen et al., 2012b). This resulted in increased vertical airflow velocity, ensuring the continuation of ascending airflow (Knaff et al., 2004). Furthermore, the thermal circulation activated by the UHI effect contributed to the sustained development and organization of the thunderstorm system. Consequently, when the thunderstorms encountered the small-scale open rise, the thermal effect enhanced the thunderstorm process, and CG events were predominantly concentrated within the built-up area.
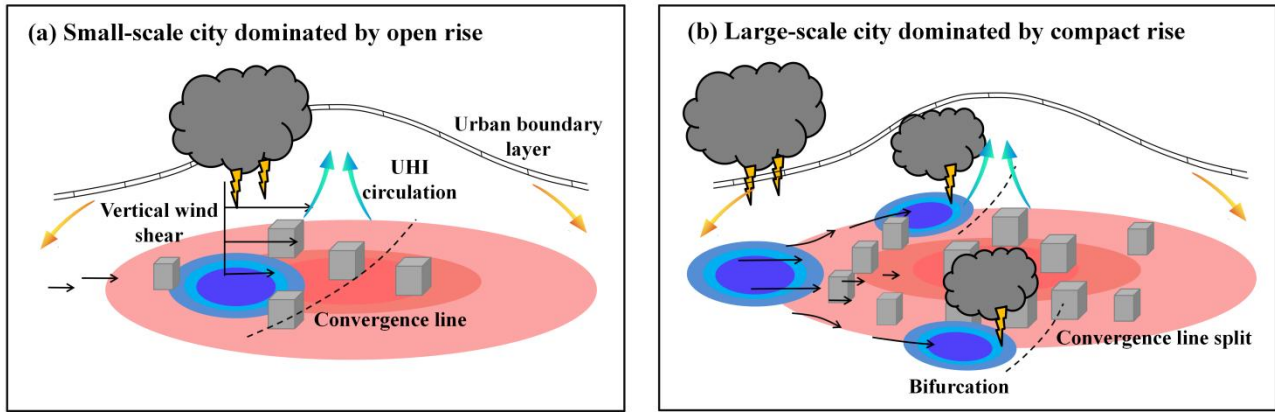
Figure 10: Schematic diagram for the modulation of (a) small-scale city dominated by open rise and (b) large-scale city dominated by compact rise on thunderstorm processes and CG activities.

As illustrated in Figure 10b, when thunderstorms passed over the large-scale city dominated by compact rise, the rough
underlying surface caused significant attenuation of the horizontal dynamic field (Jin & Shepherd, 2005; Hand & Shepherd, 2009). The urban underlying surface altered the motion state of the cold pool, leading to stagnation and accumulation at the edge of the built-up area. Once the city size and building density reach a critical threshold, the outflow of the cold pool undergoes separation, resulting in the breakdown of the convergence line. Consequently, the vertical airflow velocity above the built-up area was significantly weakened, preventing the formation of new convective cells. The propagation speed of the thunderstorm cells above the built-up area was slower than on both sides of the city, resulting in bifurcation and movement around the thunderstorm system. Certainly, as the building density increased, the barrier effect became more pronounced. Therefore, when the thunderstorm system passed over the large-scale compact rise, the barrier effect of the urban underlying surface dominated the organization process of the thunderstorm, leading to the concentrated CG events in the city periphery.

5 Conclusion

Using observation data and numerical simulations, this article conducted a detailed investigation regarding how the urban underlying surface modulates thunderstorm processes and CG activities. We first analyzed the patterns of CG activities around the Beijing megacity over eight years. Subsequently, a thunderstorm case that passed over the built-up area of Beijing megacity was selected as a representative case to investigate the potential influence of urban underlying surface on thunderstorm processes and CG activities.

Under similar climate conditions, the long-term pattern of the CG activities showed that Beijing, with its extensive city size, exhibited a notable barrier effect, while Zhangjiakou, a smaller city surrounding Beijing, did not exhibit a barrier effect. Thereafter, we counted the CG number across various LCZs, discovering that the CG density in compact rise was higher

than that in open rise. These findings suggested that city size and building density could be significant factors influencing CG activities in the built-up area. The "0713" thunderstorm passing over the Beijing megacity was selected as a representative case study. Radar echoes and AWS data revealed that the evolution of the near-surface cold pool and convergence line can provide diagnostic indicators for investigating the influence mechanisms of urban underlying surfaces on the organization process of the "0713" thunderstorm. Our simulation results further indicated that the urban underlying surface altered the motion state of the cold pool and weakened the vertical airflow within the built-up area. Notably, the strength of the barrier effect varied with city size and building density. Finally, this paper established a conceptual model that illustrated how the urban underlying surface modulated the evolution of thunderstorm processes and the pattern of CG activities.

Broadly, our findings have implications in providing an important theoretical foundation for the forecasting and early warning of urban thunderstorm disasters. In the future, we plan to conduct high-resolution observations of meteorological elements within the urban boundary layer, aiming to deeply analyze the variations in boundary layer structure, and energy balance when thunderstorms pass over the cities. Furthermore, we will design more detailed sensitivity experiments to comprehensively understand the mechanisms by which urban underlying surface impact thunderstorm disasters.

Author contributions. Tao, S., Yuanjian, Y. and Gaopeng, L. conceptualized the study. Zuofang, Z. performed the model development, conducted the simulations. Tao, S. wrote the original manuscript and plotted all the figures. Yucheng, Z., Ye, T., Lei, L., and Simone, L. assisted in the conceptualization and model development. All the authors contributed to the manuscript preparation, discussion, and writing.

Acknowledgments. The data that support the findings of this study are available from the Institute of Urban Meteorology, China Meteorological Administration and the State Grid Electric Power Research Institute, upon applying for cooperation.

Financial support. This research was funded by the National Natural Science Foundation of China (42105147, 41875006, U1938115, and 41775078), the National Key Research and Development Program (2017YFC1501501).

Competing interests. The contact author has declared that none of the authors has any competing interests.

References

Bornstein, R., and LeRoy M.: Urban barrier effect on convective and frontal thunderstorms. Preprints, Fourth Conf. on Mesoscale Processes, Boulder, CO, American Meteorological Society, 120–121, 1990.

Chen, L., Zhang, Y., Lu, W., Zheng, D., Zhang, Y., Chen, S., and Huang, Z.: Performance Evaluation for a Lightning Location System Based on Observations of Artificially Triggered Lightning and Natural Lightning, Journal of Atmospheric and Oceanic Technology, 29, 1835-1844, http://doi.org/10.1175/JTECH-D-12-00028.1, 2012a.

Chen, M., & Wang, Y.: Numerical simulation study of interactional effects of the low-level vertical wind shear with the cold pool on a squall line evolution in North China, Acta Meteorologica Sinica, 70, 3, 371–386, https://doi.org/10.11676/qxxb2012.033, 2012b.

Dai, J., Qin, H., and Zheng, J.: Analysis of lightning activity over the Yangtze River Delta using TRMM/LIS observations, Journal of Applied Meteorological Science, 16, 6, 728–736, https://doi.org/10.3969/j.issn.1001-7313.2005.06.003, 2005.

Dixon M, Wiener G.: TITAN: thunderstorm identification, tracking, analysis, and nowcasting–A radar-based methodology. Journal of Atmospheric and Oceanic Technology, 10, 785–797, https://doi.org/10.1175/1520-0426(1993)0102.0.CO;2, 1993.

Dou J., Wang, Y., Bornstein, R., and Miao, S.: Observed Spatial Characteristics of Beijing Urban Climate Impacts on Summer Thunderstorms, Journal of Applied Meteorological Science, 54, 1, 94–105, https://doi.org/10.1175/JAMC-D-13-0355.1, 2015.

Farias, W., Pinto, O., Pinto, I., and Naccarato, K.: The influence of urban effect on lightning activity: Evidence of weekly cycle, Atmospheric Research, 135-136(jan.), 370–373, https://doi.org/10.1016/j.atmosres.2012.09.007, 2014.

Hand, L. M., Shepherd, J. M.: An investigation of warm-season spatial rainfall variability in Oklahoma city: possible linkages to urbanization and prevailing wind, Journal of Applied Meteorology And Climatology, 48, 2, 251–269, https://doi.org/10.1175/2008JAMC2036.1, 2009.

He, X., Li, Y., Wang, X., Chen, L., Yu, B., Zhang, Y.: High-resolution dataset of urban canopy parameters for Beijing and its application to the integrated WRF/Urban modelling system. Journal of cleaner production, 208, 373–383, https://doi.org/10.1016/j.jclepro.2018.10.086, 2019.

Janjic, Z.: The step-mountain eta coordinate model: further developments of the convection, viscous sublayer, and turbulence closure schemes, Monthly Weather Review, 122, 927–945, https://doi.org/10.1175/1520-0493(1994)1222.0.CO;2, 1994.

Jin, M. L., Shepherd, J. M.: Inclusion of urban lands CAPE in a climate model: how can satellite data help?, Bulletin of the American Meteorological Society, 86, 681–689, https://doi.org/10.1175/BAMS-86-5-681, 2005.

Knaff, J. A., Seseske, S. A., Demaria, J. L., and Demuth, J. L.: On the influences of vertical wind shear on symmetric tropical cyclone structure derived from AMSU, Monthly Weather Review, 132, 10, 2503–2510, https://doi.org/10.1175/1520-0493(2004)1322.0.CO;2, 2004.

Kusaka, H., H. Kondo, Y. Kikegawa, & F. Kimura.: A simple single-layer urban canopy model for atmospheric models: Comparison with multi-layer and slab models. Bound. Layer Meteorol., 101, 329–358, https://doi.org/10.1023/A:10192079230782001, 2001.

Lacono, M., Delamere, J., Mlawer, E., Shephard, M. W., And, S. A. C., and Collinset, W. D.: Radiative forcing by long-lived greenhouse gases: calculations with the AER radiative transfer models, Journal of Geophysical Research-Atmospheres, 113, D13103, https://doi.org/10.1029/2008JD009944, 2008.

Lim, K., and Hong, S.: Development of an effective double-moment cloud microphysics scheme with prognostic cloud condensation nuclei (CCN) for weather and climate models, Monthly Weather Review, 138, 1587–1612, https://doi.org/10.1175/2009MWR2968.1, 2010.

Lorenz, J. M., Kronenberg, R., Bernhofer, C., and Niyogi, D.: Urban rainfall modification: observational climatology over Berlin, Germany, Journal of Geophysical Research: Atmospheres, 124, 2, 731–746, https://doi.org/10.1029/2018JD028858, 2019.

Kingfield, D. M., Calhoun, K. M., de Beurs, K. M., Henebry, G. M.: Effects of city size on thunderstorm evolution revealed through a multiradar climatology of the central United States, Journal of Applied Meteorology and Climatology, 57, 295–317, https://doi.org/10.1175/JAMC-D-16-0341.1, 2018.

Mecikalski, J. R., Bedka, K. M.: Forecasting convective initiation by monitoring the evolution of moving cumulus in daytime GOES imagery. Monthly Weather Review, 134, 49–78, https://doi.org/10.1175/MWR3062.1, 2006.

Melin, H., Bormin, H., and Hung-Lung, A. H.: Acceleration of the WRF Monin-Obukhov-Janjic surface layer parameterization scheme on an MIC-based platform for weather forecast, IEEE Journal of Selected Topics in Applied Earth Observations and Remote Sensing, 10, 4399–4408, https://doi.org/10.1109/JSTARS.2017.2725743, 2017.

Miao, S., Chen, F., Li, Q., and Fan, S.: Impacts of urban processes and urbanization on summer precipitation: a case study of heavy rainfall in Beijing on August 1st 2006, Journal of Applied Meteorology and Climatology, 50, 4, 806–825, https://doi.org/10.1175/2010JAMC2513.1, 2011.

National Bureau of Statistics of the People's Republic of China: China statistical yearbook 2021, Beijing, China Statistics Press, 2021.

Orville, R. E., Huffines, G. R., Burrows, W. R., Holle, R. L., and Cummins, K. L.: The north American lightning detection network (NALDN)-first results: 1998-2002, Monthly Weather Review, 130, 2098–2109, https://doi.org/10.1175/1520-0493(2002)130<2098:TNALDN>2.0.CO;2, 2002.

Pinto, I.R.C.A., Pinto, O., Rocha, R.M.L., Diniz, J.H., Carvalho, A.M., and Filho, A.C.: Cloud-to-ground lightning in southeastern Brazil in 1993: Time variations and flash characteristics, Journal of Geophysical Research: Space Physics, 104, 31381–31387, https://doi.org/10.1029/1999JD900799, 1999.

Qie, X., Yuan, S., Chen, Z., Wang, D., Liu, D., Sun, M., Sun, Z., Srivastava, A., Zhang, H., Lu, J., Xiao, H., Bi, Y., Feng, L., Tian, Y., Xu, Y., Jiang, R., Liu, M., Xiao, X., Duan, S., Su, D., Sun, C., Xu, W., Zhang, Y., Lu, G., Zhang, D., Yin, Y., and Yu, Y.: Understanding the dynamical-microphysical-electrical processes associated with severe thunderstorms over

450   the Beijing metropolitan region, Science China Earth Sciences, 64, 1, 1–17, http://doi.org/10.1007/s11430-020-9656-8, 2021.

Roberts, R. D., Rutledge, S.: Nowcasting storm initiation and growth using GOES-8 and WSR-88D data. Weather and Forecasting, 18, 562–584, https://doi.org/10.1175/1520-0434(2003)0182.0.CO;2, 2003.

Schulz, W., Cummins, K., Diendorfer, G., Dorninger, M.: Cloud-to-ground lightning in Austria: A 10-year study using data
455   from a lightning location system, Journal of Geophysical Research: Space Physics, 110, D9, D09101, https://doi.org/10.1029/2004JD005332, 2005.

Shepherd, J. M.: A review of current investigations of urban-induced rainfall and recommendations for the future, Earth Interactions, 9, 1-27 https://doi.org/10.1175/EI156.1, 2005.

Shi, T., Yang, Y., Liu, L., Tian, Y., Zheng, Z., Huang, Y., Xiao, Z., Wang, Y., Wang, Y., Lu, G.: Spatiotemporal patterns of
460   long series of cloud-to-ground lightning in Beijing and its cause, Urban Climate, 49, 101480, https://doi.org/10.1016/j.uclim.2023.101480, 2023.

Stallins, J. A., and Bentley, M. L.: Urban lightning climatology and GIS: An analytical framework from the case study of Atlanta, Georgia, Applied Geography, 26, 3–4, 242–259, https://doi.org/10.1016/j.apgeog.2006.09.008, 2006.

Stewart, I. D., and Oke, T. R.: Local Climate Zones for Urban Temperature Studies, Bulletin of the American
465   Meteorological Society, 93, 12, 1879–1897, http://doi.org/10.1175/BAMS-D-11-00019.1, 2012.

Sun, J., and Yang, B.: Meso-β Scale Torrential Rain Affected by Topography and the Urban Circulation, Chinese Journal of Atmospheric Sciences, 32, 6, 1352–1364, https://doi.org/10.3878/j.issn.1006-9895.2008.06.10, 2008.

Sun, J., He, N., Guo, R., and Chen, M.: The Configuration Change and Train Effect Mechanism of Multi-Cell Storms, Chinese Journal of Atmospheric Sciences, 37, 1, 137–148, https://doi.org/CNKI:SUN:DQXK.0.2013-01-014, 2013.

470   Sun, X., Luo, Y., Gao X., Wu, X., and Xu, H.: On the Localized Extreme Rainfall over the Great Bay Area in South China with Complex Topography and Strong UHI Effects, Monthly Weather Review, 149, 8, 2777–2801, https://doi.org/10.1175/MWR-D-21-0004.1, 2021.

Takemi, T.: Impacts of moisture profile on the evolution and organization of mid-latitude squall lines under various shear conditions, Atmospheric Research, 82, 1-2, 37–54, https://doi.org/10.1016/j.atmosres.2005.01.007, 2006.

475   Tewari, M., Chen, F., Wang, W., Dudhia, J., and Cuenca, H.: Implementation and verification of the unified NOAH land surface model in the WRF model, 20th conference on weather analysis and forecasting/16th conference on numerical weather prediction, pp.11–15, 2004.

Wang, Q., Li, Zb., Guo, J., Zhao, C., and Cribb, M.: The climate impact of aerosols on the lightning flash rate: Is it detectable from long-term measurements?, Atmospheric Chemistry Physics, 18, 17, 12797–12816,
480   https://doi.org/10.5194/acp-18-12797-2018, 2018.

Wang, Y., Lu, G., Shi, T., Ma, M., and Wang, Y.: Enhancement of Cloud-to-Ground Lightning Activity Caused by the Urban Effect: A Case Study in the Beijing Metropolitan Area, Remote Sensing, 13, 7, 1228, https://doi.org/10.3390/rs13071228, 2021.

Steiger, S. M., Orville, R. E.: Cloud-to-ground lightning characteristics over Houston, Texas: 1989-2000, Journal of Geophysical Research-Space Physics, 107, D11, https://doi.org/10.1029/2001jd001142, 2002.

Weisman, M. L., and Klemp, J. B.: The structure and classification of numerically simulated convective storms in directionally varying wind shears, Monthly Weather Review, 112, 12, 2479–2498, https://doi.org/ 10.1175/1520-0493(1984)112<2479:TSACON>2.0.CO;2, 1984.

Westcott, N. E.: Summertime Cloud-to-Ground Lightning Activity around Major Midwestern Urban Areas, Journal of Applied Meteorology, 34, 7, 1633–1642, https://doi.org/10.1175/1520-0450-34.7.1633, 1995.

Xiao, X., Sun, J., Chen, M., Qie, X., and Ying, Z.: The characteristics of weakly forced mountain-to-plain precipitation systems based on radar observations and high-resolution reanalysis, Journal of Geophysical Research-Atmospheres, 122, 6, 3193–3213, https://doi.org/10.1002/2016JD025914, 2017.

Xu, R., Miao, J., and Tan, Z.: Numerical Simulation of the Impact of Urban Underlying Surface Characteristics on Thunderstorm in Nanjing, Chinese Journal of Atmospheric Sciences, 37, 6, 1235–1246, https://doi.org/10.3878/j.issn.1006-9895.2012.12128, 2013.

Yang, L., Li, Q., Yuan, H., Niu, Z., and Wang, L.: Impacts of urban canopy on two convective storms with contrasting synoptic conditions over Nanjing, China, Journal of Geophysical Research: Atmospheres, 126, 9, e2020JD034509, https://doi.org/10.1029/2020JD034509, 2021.

Yang, P., Liu, W.D., Zhong, J.Q., Yang, J. Evaluating the Quality of Temperature Measured at Automatic Weather Stations in Beijing, Journal of Applied Meteorological Science, 22, 6, 706–715, https://doi.org/1001-7313(2011)22:6<706:BJDQZD>2.0.TX;2-2 , 2011.

Yin, J., Zhang, D., Luo, Y., and Ma, R.: On the Extreme Rainfall Event of May 7th 2017 Over the Coastal City of Guangzhou. Part I: Impacts of Urbanization and Orography, Monthly Weather Review, 148, 3, 955–979, https://doi.org/10.1175/MWR-D-19-0212.1, 2020.

Yuan, Z.: Study of the influence of the different horizontal resolutions and microphysical setups on the idealized simulation of a squall line, Acta Meteorologica Sinica, 73, 4, 648–666, https://doi.org/10.11676/qxxb2015.049, 2015.

Yue, C., Tang, Y., Gu, W., Han, Z., and Wang, X.: Study of Urban barrier effect on Local Typhoon Precipitation, Meteorological Monthly, 45, 11, 1611–1620, https://doi.org/CNKI:SUN:QXXX.0.2019-11-011, 2019.

Zhu, Y., Liu, H., and Shen, J.: Influence of Urban Heat Island on Pollution Diffusion in Suzhou, Plateau Meteorology, 35, 6, 1584–1594, https://doi.org/10.7522/j.issn.1000-0534.2016.00084, 2016.